PEDIATRIC

Persefoni N. Margariti
Konstantinos Blekas
Frosso G. Katzioti
Anastasia K. Zikou
Meropi Tzoufi
Maria I. Argyropoulou

Magnetization transfer ratio and volumetric analysis of the brain in macrocephalic patients with neurofibromatosis type 1

P. N. Margariti · F. G. Katzioti ·
A. K. Zikou · M. I. Argyropoulou (✉)
Department of Radiology,
Medical School,
University of Ioannina,
Ioannina, Greece
e-mail: margyrop@cc.uoi.gr
Tel.: +30-2651-97733
Fax: +30-2651-97862

K. Blekas
Department of Computer Science,
University of Ioannina,
Ioannina, Greece

M. Tzoufi
Child Health Department,
Medical School,
University of Ioannina,
Ioannina, Greece

Abstract The purpose of the study was to evaluate brain myelination by measuring the magnetization transfer ratio (MTR) and to measure grey (GMV) and white matter volume (WMV) in macrocephalic children with neurofibromatosis type 1 (NF1). Seven NF1 patients (aged 0.65–16.67 years) and seven age- and gender-matched controls were studied. A three-dimensional (3D) gradient echo sequence with and without magnetization transfer (MT) prepulse was used for MTR assessment. Volume measurements of GM and WM were performed by applying segmentation techniques on T2-weighted turbo spin echo images (T2WI). MTR of unidentified bright objects (UBOs) on T2WI in cerebellar white matter (52.8±3.3), cerebral peduncles (48.5±1.5), hippocampus (52.6±1.1), internal capsule (55.7±0.3), globus pallidus (52.7±3.9), and periventricular white matter (52.6±1.2) was lower than in the corresponding areas of controls (64.6±2.5, 60.8±1.3, 56.4±0.9, 64.7±1.9, 59.2±2.3, 63.6±1.7, respectively; $p<0.05$). MTR of normal-appearing brain tissue in patients was not significantly different than in controls. Surface area (mm^2) of the corpus callosum (809.1±62.8), GMV (cm^3) (850.7±42.9), and white matter volume (WMV) (cm^3) (785.1±85.2) were greater in patients than in controls (652.5±52.6 mm^2, 611.2±92.1 cm^3, 622.5±108.7 cm^3, respectively; $p<0.05$). To conclude, macrocephaly in NF1 patients is related to increased GMV and WMV and corpus callosum enlargement. MTR of UBOs is lower than that of normal brain tissue.

Keywords Magnetization transfer ratio · Grey matter volume · White matter volume · Neurofibromatosis type 1 · Corpus callosum

Introduction

Neurofibromatosis type 1 (NF1) is an autosomal dominant disorder characterized by prominent cutaneous manifestations and central nervous system (CNS) lesions [1]. Hyperintense signal alterations on T2-weighted images, called unidentified bright objects (UBOs), are the hallmark of the disease in the brain [2, 3]. Although the nature and significance of the UBOs remains obscure, there is evidence that these lesions are part of a more diffuse brain disorder [3, 4]. Indeed, in some studies, higher numbers of UBOs have been reported in NF1 patients with macrocephaly and learning disabilities [5, 6]. Magnetic resonance imaging (MRI) using quantitative morphometric analysis revealed increased size of the corpus callosum (CC) and greater grey matter volume (GMV) [5]. Nevertheless, other studies have demonstrated an enlargement in white matter volume (WMV) [7, 8].

MR spectroscopy, which provides information on neuronal/axonal viability, cellular membrane integrity, and cellular energetics, has been used for the evaluation of patients with NF1 and demonstrated abnormalities in brain

metabolites, such as increases in choline and decreases in N-acetyl aspartate [9]. Diffusion-weighted imaging (DWI), which detects changes of random motion of water molecules and provides information about tissue microscopic barriers, has been used for the evaluation of UBOs and normal-appearing (NA) brain tissue [4, 10, 11]. Although increased apparent diffusion coefficient (ADC) values have been found in UBOs, there is disagreement regarding ADC values of the NA thalamus and globus pallidus [4, 10, 11].

A technique that can shed further light on NF1 pathology is magnetization transfer (MT) imaging. MT is based on interactions between macromolecular and free water protons of tissue [12]. For MT imaging, an on-resonance or off-resonance radiofrequency prepulse is applied before a spin echo or gradient echo sequence to saturate preferentially the restricted protons [12, 13]. While the restricted macromolecular protons are held in a state of saturation, the equilibrium longitudinal magnetization of the free water protons decreases exponentially to a lower value with a new lower time constant (T1sat) [12, 13]. Efficacy of the MT phenomenon is evaluated by measuring the magnetization transfer ratio (MTR) [12, 13]. MTR is determined by field strength and scanning parameters but principally by concentration of macromolecules and efficacy of interaction between the bound and free pools of protons 13]. MTR has never been used for evaluation of NF1.

In the present study, we sought to determine whether MTR values of UBOs and NA brain tissue in NF1 patients differ from said values in healthy controls. Furthermore, intracranial brain volume, GMV, WMV, and area of the CC were calculated using morphometric analysis of MR images and subsequently compared with corresponding variables in healthy controls.

Materials and methods

Brain MR examinations of seven children (three girls, four boys; mean age 11.1 years, range 0.65–16.67 years) with NF1 as defined by clinical diagnostic criteria outlined by the National Institutes of Health [1] were retrospectively evaluated and compared with those of seven age- and gender-matched healthy controls. Control subjects were screened for either headache or suspicion of meningoencephalitis and had normal brain MRI. Fronto-occipital circumference assessed systematically before MRI was within normal for age values in controls while all NF1 patients were found to be macrocephalic (fronto-occipital circumference greater than +2SD compared with normal for age values) [14].

All MR examinations were performed on the same 1.5-T MR unit (Gyroscan ACS NT; Philips Medical Systems, Best, The Netherlands) using a head coil, field of view of 24 cm, and 256×256 acquisition matrix. Sequences were: axial T2-weighted turbo spin echo (TR/TE 3500/90; slice

thickness 5 mm; intersection gap 0 mm); coronal T2-weighted turbo spin echo (TR/TE 3500/90; slice thickness 2.5 mm; intersection gap 0 mm); sagittal plain T1-weighted spin echo (TR/TE 650 /17 ms; slice thickness 4 mm; intersection gap 0.4 mm); and contrast-enhanced axial, coronal, and sagittal T1-weighted spin echo. Area measurement of the CC was performed in a midline sagittal scan of the plain T1-weighted sequence. As a strict midline sagittal plane was considered an image depicting simultaneously the CC, anterior and posterior lobes, the stalk of the pituitary gland, and the aqueduct of Sylvius. CC was discriminated from the surrounding tissues by its characteristic morphology and higher signal. Measurement was obtained using the cursor of the machine by freehand outline of the CC. Axial T2-weighted sequence was used for intracranial brain tissue (IBT), WMV, GMV, and cerebrospinal fluid volume (CSFV) measurements. This sequence was chosen because it covered the entire intracranial volume, and the slices were contiguous. Moreover, this sequence provided a good GM–WM contrast of the myelinated brain in the six patients and controls older than 5 years. In the two infants (one patient and one control aged 0.65 years), the contrast between grey matter and the largely unmyelinated, at this age, WM was also satisfactory. Segmentation was performed with a home-made software package developed by one author (KB) of the IPAN group http://www.cs.uoi.gr/~ipan who is specialized in image processing, analysis, and modelling. The following steps were executed for each patient's study:

1. Image data (in DICOM format) were accessed and read.
2. An operator (PNM) outlined intracranial structures, and a (binary) mask was created in order to separate background and bone from the useful information of the image.
3. The resulting T2-weighted images were segmented automatically in order to group together image pixels based only on their intensity values. Clustering based only on intensity values was used for this image segmentation task [15]. More specifically, the k-means algorithm was used [16]. This algorithm iterates between adjusting the cluster centers in order to minimize the distance from each data point to its nearest center and labels the data points based on their closest centers. One issue that needs to be addressed is the number of clusters that will be used. We observed that the number of clusters that best captured the spatial distribution of WM), GM, and CSF was five. This is explained because the spatial distribution of WM and GM is best captured if two clusters are used for each. Therefore, we applied the k-means algorithm using as data points the pixels obtained from the masked images using k=5 for the number of clusters. After finishing with clustering, we merged the two clusters with the smallest intensities to form the WM cluster and the two

clusters with intermediate intensities to form the GM cluster. The remaining cluster with the highest level of pixel intensity values represented CSF.

4. After finishing the clustering process, WMV, GMV, and CSFV measurements were obtained by multiplying the total number of pixels of the corresponding WM, GM, and CSF clusters, respectively, with pixel size and slice thickness. IBT was calculated by adding WMV and GMV.

To study the MT phenomenon, a three-dimensional (3D) gradient echo sequence (TR/TE 32/8, flip angle 6°) was performed, and 4-mm/2-mm overlapping sections were concurrently obtained both with and without the application of MT binomial prepulse applied on-resonance. Images of this sequence obtained before application of MT prepulse had proton-density contrast due to the short TE and small flip angle (Fig. 1a). The MT sequence performed in the axial plane (perpendicular to the intercommisural line, i.e., the anterior commissure to posterior commissure line, or AC-PC line) was part of our standard protocol. Images obtained after application of the MT prepulse depict structures of high MTR with low signal intensity and those of low MTR with higher intensity (Fig. 1b). The duration of a complete MR examination ranged from 15 to 25 min. MTRs were calculated from circular regions of interest (ROIs), with a minimum size of 0.5 mm^2. In all cases, UBOs observed on T2-weighted images were also detectable in proton density images of the MT sequence; therefore, ROIs were positioned at an image without MT and copy–pasted to the corresponding image with MT. Signal intensity measurements were performed bilaterally in the following regions: cortex and WM of the frontal and occipital lobe, caudate nucleus, putamen, globus pallidus, thalamus, optic chiasm, internal capsule, genu and splenium of the CC, hippocampus, cerebral peduncles, and cerebellar WM. Care was taken to avoid the partial volume effect of CSF when defining ROIs. MTR

was calculated as: $(SI_0-SI_m)/SI_0 \times 100\%$ where SI_0 is the signal intensity from the image acquired without a MT prepulse and SI_m refers to signal intensity from an image acquired with MT prepulse.

Statistical analysis

Data analysis was carried out using SPSS base 13 for Windows. Normality of the distribution of parameters was assessed by the Kolmogorov-Smirnov test. Unpaired two-tailed Student's t test was used to study differences between patients and controls. A p value <0.05 was considered significant.

Results

UBOs in T2-weighted images lacking mass effect and enhancement after contrast infusion, compatible with "hamartomas," were observed in the globus pallidus (6/7 patients), cerebral peduncles (3/7), periventricular WM (2/7), internal capsule (2/7), cerebellar WM (2/7), and hippocampus (1/7). Optic chiasm glioma appearing hyperintense in T2-weighted images and heterogeneously enhancing after contrast administration was observed in one patient. There was no significant difference in MTR values of normal-appearing GM and WM structures between patients and controls (Table 1). MTR of optic chiasm glioma (56.6) was lower compared with MTR of normal WM in controls (63.6±1.7). MTR values of UBOs in the different anatomic locations were significantly lower compared with MTRs of the corresponding normal-appearing anatomic regions in patients and controls (Table 1). The area of CC, WMV, GMV, and IBT were significantly larger in patients compared with controls (Table 2). There was no significant difference in CSFV between patients and controls (Table 2).

Fig. 1 A 14-year-old boy with lesions in the right and left globus pallidus (arrows) a Axial proton-density magnetic resonance (MR) image before application of the magnetization transfer (MT) prepulse. b After application of MT prepulse
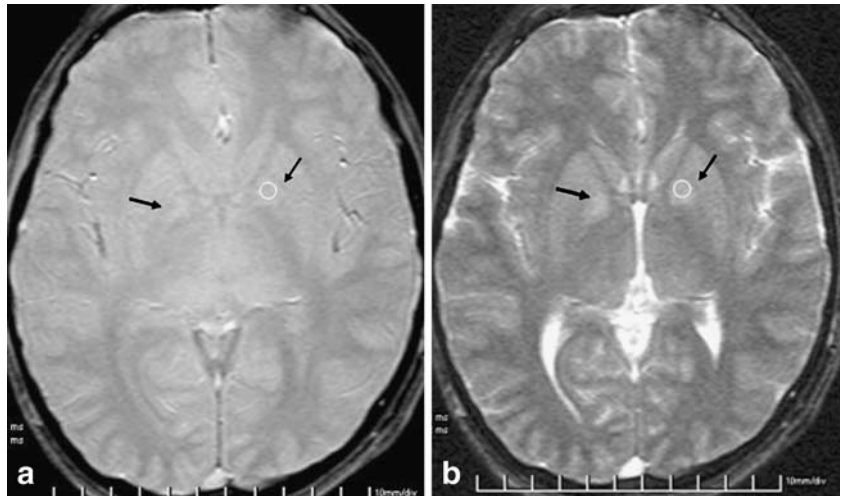
Table 1 Comparison of magnetization transfer ratio (MTR) (means± SD) of normal-appearing regions (NA) and unidentified bright objects (UBOs) in neurofibromatosis type 1 (NF1) patients with MTR of corresponding regions in controls

	Patients	Controls	p value
Frontal white matter			
NA	63.1±5.4	64.8±5.1	NS
Occipital white matter			
NA	63.0±5.5	64.5±2.2	NS
Frontal grey matter			
NA	57.4±4.3	57.3±2.4	NS
Occipital grey matter			
NA	56.5±6.2	57.5±2.9	NS
Caudate nucleus			
NA	56.6±3.0	56.5±1.7	NS
Putamen			
NA	56.5±4.2	57.2±1.8	NS
Thalamus			
NA	57.9±2.1	59.2±3.2	NS
Genu corpus callosum			
NA	64.1±5.9	65.6±3.7	NS
Splenium corpus callosum			
NA	67.9±5.6	66.9±3.7	NS
Optic chiasm			
NA	62.5±3.3	63.0±3.9	NS
Optic glioma[a]	56.6*	63.0±3.9	
Periventricular white matter			
NA	62.9±4.2	63.6±1.7	NS
UBOs	52.6±1.2	63.6±1.7	<0.01
Globus pallidus			
NA	58.9±1.9	59.2±2.3	NS
UBOs	52.7±3.9	59.2±2.3	<0.01
Internal capsule			
NA	62.9±4.3	64.7±1.9	NS
UBOs	55.7±0.3	64.7±1.9	<0.01
Hippocampus			
NA	56.0±1.0	56.4±0.9	NS
UBOs	52.6±1.1	56.4±0.9	<0.05
Cerebral peduncles			
NA	60.6±1.0	60.8±1.3	NS
UBOs	48.5±1.5	60.8±1.3	<0.01
Cerebellar white matter			
NA	63.9±3.3	64.6±2.5	NS
UBOs	52.8±3.3	64.6±2.5	<0.01

NA normal appearing, *NS* not significant, *HYSA* , *UBOs* unidentified bright objects

[a]One case of optic glioma

Discussion

MT imaging offers tissue contrast depending on the presence of restricted macromolecular protons [12]. These protons, although "invisible" in classic MR sequences, indirectly affect image contrast by exchanging longitudinal magnetization with free water protons [12, 13, 17, 18]. MT techniques preferentially saturate the restricted protons by using either an on-resonance or off-resonance radiofrequency prepulse since the latter have a broad spectral line compared with free water protons [12, 13, 17, 18]. There is evidence that MT contrast in the brain is mainly related to the presence of myelin since experimental studies have demonstrated that the MT effect for myelin water is much larger than for intra- or intercellular water [19]. These techniques have been largely used for evaluation of the myelination process and for the study of demyelinating disorders [13, 17, 18, 20, 21]. As regards phakomatoses, only tuberous sclerosis has been studied using the MT technique. In this disorder, MTR abnormalities were not only detected in cortical tubers and subependymal nodules but also in NA WM [22]. In the present study, brain MTR was evaluated in a series of NF1 patients, and a low MTR was found in UBOs, suggesting hypomyelination or abnormal myelin structure. Indeed, abnormal myelin with fluid-filled vacuoles has been histologically detected in UBOs [2]. Myelin abnormalities are also found at the periphery of tumefactive multiple sclerosis lesions, and MTR values reported in these areas in a previous study are similar to those we found in WM UBOs [23]. It is worth pointing out that in the previous study, assessment of MTR was performed with the same MR sequence we used in the present study [23]. Myelin abnormalities in UBOs may also account for the high ADC values assessed in DWI since pathologic processes that alter tissue organization by changing the number and permeability of barriers cause abnormal tissue diffusivity [11].

An MTR lower than that of normal WM and chiasm was also found in the one chiasmatic glioma evaluated in this study. This finding is in agreement with previously reported data demonstrating that gliomas, particularly low-grade ones, have lower MTRs and higher ADCs than normal WM [24, 25]. Moreover, the study of Pui et al. [25], which focused on DWI and MT imaging to evaluate solid brain tumors in a series of 37 pediatric patients, demonstrated that ADC increased and MTR decreased with lower tumor grade. Nevertheless, in a case report of an 1-year-old NF1 patient with optic nerve and chiasmatic glioma, the reported ADC was not different from that of the WM in a control group of children aged 9 months to 3 years [26]. This absence of difference might have been rather random because in this age range, ADC, which follows a monoexponential function in the developing brain, still has a high rate of change, and therefore high and low ADC values may have been included for comparisons [27]. MT techniques are more sensitive than conventional MR sequences in detecting depleted or disordered myelination [12, 21, 22]. Indeed, a low MTR has been reported in NA WM in patients with multiple sclerosis and tuberous sclerosis [21, 22]. Optic gliomas have lower MTR than normal optic chiasm, which consists of myelinated WM

Table 2 Comparison of cerebrospinal fluid (CSF), white matter (WM), grey matter (GM), intracranial brain tissue (IBT) volume, and corpus callosum (CC) size between neurofibromatosis type 1 (NF1) patients and controls

	Patients	Controls	*p* value
CSF volume (cm^3)	85.50±23.9	60.0±14.6	NS
Grey matter volume (cm^3)	850.7±42.9	611.2±92.1	<0.001
White matter volume (cm^3)	785.1±85.2	622.5±108.7	<0.05
Intracranial brain tissue volume (cm^3)	1635.9±59.3	1233.8±155.9	<0.001
Corpus callosum size (cm^2)	809.1±62.8	652.5±52.6	<0.005

NS not significant

fibers [25, 26]. A low MTR before the detection of signal abnormalities and optic chiasm enlargement on conventional MR sequences might be a useful marker of pending optic glioma in NF1 patients. The MTR of optic glioma was within the range of MTR values assessed in UBOs of other WM areas. Further longitudinal studies are necessary to establish the value of MTR in the differential diagnosis between UBOs and neoplastic lesions.

The pathogenesis of NF has been related with inactivation of a gene encoding for neurofibromin, which is a tumor suppressor protein [28]. Experimental studies in NF1 mice demonstrated that loss of neurofibromin results in abnormal accumulation of oligodendrocyte progenitor cells [28]. Corroborating these findings, loss of neurofibromin may also account for diffuse glial proliferation in the brain of NF1 patients [2, 29]. Previous studies using DWI indicated higher ADC values in NA brain tissue of NF1 patients compared with corresponding areas in controls [4, 9, 10]. In contrast, in the present study, there was no difference between the MTR of NA brain tissue in NF1 patients and that of corresponding areas in controls. The disagreement between the present study and those using DWI probably suggests that MT and DWI provide relatively independent measures of NF1 abnormalities and that their combined use might be of value in understanding the mechanisms underlying clinical manifestations of the disease.

Macrocephaly, which occurs in up to 53% of patients with NF1, has been associated with clinical and physical severity while increased GMV has been related with learning disability [5, 8, 30]. There is disagreement among the few studies evaluating GMV and WMV in NF1 patients as to which brain region is abnormally increased [5, 7, 8]. Increase in the WMV has been reported in two studies, one of which demonstrated a tendency for GMV to be greater in macrocephalic NF1 patients than in controls [7, 8]. A third study showed that children with NF1 have larger GMV than healthy controls, and this difference persisted even when patients with optic glioma were excluded from the analysis [5]. Differences in the population under study and in MR sequence and segmentation technique used for GMV and WMV evaluation may have been partly responsible for this dissimilarity. All patients included in the present study had significantly larger GMV, WMV, and IBT volume compared with controls, suggesting that macrocephaly is due to megencephaly. Moreover, in agreement with previous studies, we found a larger CC surface area in patients than in controls [5, 31].

Although the pathogenesis of macrocephaly in NF1 remains uncertain, an anomaly of the normal developmental process of myelination seems to be the most attractive theory at present [5, 7, 31]. The myelin sheath, which is wrapped in spiral fashion around the axon, consists of modified extensions of oligodendroglial cell processes [32]. Experimental studies have demonstrated in the spinal cord of NF1 mice dramatically increased numbers of CNS oligodendrocyte progenitor cells, which have the ability to form oligodendrocytes after in vivo transplantation [24]. Accordingly, increased numbers of oligodendrocyte progenitor cells or even of oligodendrocytes in the GM and WM of NF1 patients might be suggested as an underlying cause for megencephaly. Another possible mechanism for increased brain volume in NF1 patients might be a lack of axonal elimination due to a defective mechanism of apoptosis [30]. Indeed, activation of Ras proteins, which protect some cells from apoptosis, is regulated by neurofibromin [33, 34]. If apoptotic axonal elimination occurs in humans as it does in rhesus monkeys, neurofibromin might be responsible for megencephaly in NF1 patients by regulating the Ras pathway [35].

A potential limitation of the study is that the slice thickness of the axial T2-weighted sequence was not optimum for volumetric assessment.

To conclude, macrocephaly in NF1 patients is due to megencephaly. MT techniques, by detecting low MTR in UBOs and optic chiasm gliomas, may be useful in the diagnostic workup of NF1 patients.

References

1. NIH (1988) National Institutes of Health consensus development conference. Neurofibromatosis conference statement. Arch Neurol 45:575–578

2. DiPaolo DP, Zimmerman RA, Rorke LB, Zackai EH, Bilaniuk LT, Yachnis AT (1995) Neurofibromatosis type 1: pathologic substrate of high-signal-intensity foci in the brain. Radiology 195:721–724

3. Mentzel HJ, Seidel J, Fitzek C, Eichhorn A, Vogt S, Reichenbach JR, Zintl F, Kaiser WA (2005) Pediatric brain MRI in neurofibromatosis type I. Eur Radiol 15:814–822

4. Eastwood JD, Fiorella DJ, MacFall JF, Delong DM, Provenzale JM, Greenwood RS (2001) Increased brain apparent diffusion coefficient in children with neurofibromatosis type 1. Radiology 219:354–358

5. Moore BD 3rd, Slopis JM, Jackson EF, De Winter AE, Leeds NE (2000) Brain volume in children with neurofibromatosis type 1: relation to neuropsychological status. Neurology 54:914–920

6. North K, Joy P, Yuille D, Cocks N, Mobbs E, Hutchins P, McHugh K, de Silva M (1994) Specific learning disability in children with neurofibromatosis type 1: significance of MRI abnormalities. Neurology 44:878–883

7. Steen RG, Taylor JS, Langston JW, Glass JO, Brewer VR, Reddick WE, Mages R, Pivnick EK (2001) Prospective evaluation of the brain in asymptomatic children with neurofibromatosis type 1: relationship of macrocephaly to T1 relaxation changes and structural brain abnormalities. AJNR Am J Neuroradiol 22:810–817

8. Said SM, Yeh TL, Greenwood RS, Whitt JK, Tupler LA, Krishnan KR (1996) MRI morphometric analysis and neuropsychological function in patients with neurofibromatosis. Neuroreport 7:1941–1944

9. Jones AP, Gunawardena WJ, Coutinho CM (2001) 1H MR spectroscopy evidence for the varied nature of asymptomatic focal brain lesions in neurofibromatosis type 1. Neuroradiology 43:62–67

10. Alkan A, Sigirci A, Kutlu R, Ozcan H, Erdem G, Aslan M, Ates O, Yakinci C, Egri M (2005) Neurofibromatosis type 1: Diffusion weighted imaging findings of brain. Eur J Radiol 56:229–234

11. Tognini G, Ferrozzi F, Garlaschi G, Piazza P, Patti A, Virdis R, Bertolino C, Bertolino G, Manfredini D, Zompatori M, Crisi G (2005) Brain apparent diffusion coefficient evaluation in pediatric patients with neurofibromatosis type 1. J Comput Assist Tomogr 29:298–304

12. Grossman RI, Gomori JM, Ramer KN, Lexa FJ, Schnall MD (1994) Magnetization transfer: theory and clinical applications in neuroradiology. Radiographics 14:279–290

13. Mehta RC, Pike GB, Enzmann DR (1995) Magnetization transfer MR of the normal adult brain. Am J Neuroradiol 16:2085–2091

14. Jones KL (1997) Smith's recognizable patterns of human malformation, 5th edn. WB Saunders Co, Philadelphia

15. Pal NR, Pal SK (1993) A review of image segmentation techniques. Pattern Recognition 26:1277–1294

16. Duda RO, Hart PE, Stork DG (2001) Pattern classification, 2nd edn. Wiley-Interscience, New York

17. Engelbrecht V, Rassek M, Preiss S, Wald C, Modder U (1998) Age-dependent changes in magnetization transfer contrast of white matter in the pediatric brain. Am J Neuroradiol 19:1923–1929

18. Xydis V, Astrakas L, Zikou A, Pantou K, Andronikou S, Argyropoulou MI (2006) Magnetization transfer ratio in the brain of preterm subjects: age-related changes during the first 2 years of life. Eur Radiol 16(1):215–220

19. Stanisz GJ, Kecojevic A, Bronskill MJ, Henkelman RM (1999) Characterizing white matter with magnetization transfer and T(2). Magn Reson Med 42:1128–1136

20. Vavasour IM, Whittall KP, MacKay AL, Li DK, Vorobeychik G, Paty DW (1998) A comparison between magnetization transfer ratios and myelin water percentages in normals and multiple sclerosis patients. Magn Reson Med 40:763–768

21. Richert ND, Frank JA (1999) Magnetization transfer imaging to monitor clinical trials in multiple sclerosis. Neurology 53(5 Suppl 3):S29–S32

22. Zikou A, Ioannidou MC, Tzoufi M, Astrakas L, Argyropoulou MI (2005) Magnetization transfer ratio measurements of the brain in children with tuberous sclerosis complex. Pediatr Radiol 35:1071–1074

23. Metafratzi Z, Argyropoulou MI, Tzoufi M, Papadopoulou Z, Efremidis SC (2002) Conventional MRI and magnetisation transfer imaging of tumour-like multiple sclerosis in a child. Neuroradiology 44:97–99

24. Kurki T, Lundbom N, Komu M, Kormano M (1996) Tissue characterization of intracranial tumors by magnetization transfer and spin-lattice relaxation parameters in vivo. J Magn Reson Imaging 6:573–579

25. Pui MH, Wang Y (2005) Diffusion and magnetization transfer MRI of brain infarct, infection, and tumor in children. Clin Imaging 29:162–171

26. Sener RN (2002) Diffusion MRI in neurofibromatosis type 1: ADC evaluations of the optic pathways, and a comparison with normal individuals. Comput Med Imag Graph 26:59–64

27. Engelbrecht V, Scherer A, Rassek M, Witsack HJ, Modder U (2002) Diffusion-weighted MR imaging in the brain in children: findings in the normal brain and in the brain with white matter diseases. Radiology 222:410–418

28. Bennett MR, Rizvi TA, Karyala S, McKinnon RD, Ratner N (2003) Aberrant growth and differentiation of oligodendrocyte progenitors in neurofibromatosis type 1 mutants. J Neurosci 23:7207–7217

29. Nordlund ML, Rizvi TA, Brannan CI, Ratner N (1995) Neurofibromin expression and astrogliosis in neurofibromatosis (Type 1) brains. J Neuropathol Exp Neurol 54:588–600

30. Zvulunov A, Weitz R, Metzker A (1998) Neurofibromatosis type 1 in childhood: evaluation of clinical and epidemiologic features as predictive factors for severity. Clin Pediatr 37:295–299

31. Dubovsky EC, Booth TN, Vezina G, Samango-Sprouse CA, Palmer KM, Brasseux CO (2001) MR imaging of the corpus callosum in pediatric patients with neurofibromatosis type 1. AJNR Am J Neuroradiol 22:190–195

32. Barkovich AJ (2000) Concepts of myelin and myelination in neuroradiology. AJNR Am J Neuroradiol 21:1099–1109

33. Rosenbaum T, Kim HA, Boissy YL, Ling B, Ratner N (1999) Neurofibromin, the neurofibromatosis type 1 Ras-GAP, is required for appropriate P0 expression and myelination. Ann N Y Acad Sci 883:203–214

34. Downward J (1998) Ras signalling and apoptosis. Curr Opin Genet Dev 8:49–54

35. LaMantia AS, Rakic P (1990) Axon overproduction and elimination in the corpus callosum of the developing rhesus monkey. J Neurosci 10:2156–2175